J Supercond Nov Magn (2018) 31:547–559
DOI 10.1007/s10948-017-4211-5

ORIGINAL PAPER

# The Effects of Ru and Rh Substitutions on the Magneto-electronic and Optical Properties of the $TbNi_5$ Intermetallic Compound: An Ab Initio Investigation

**Mohammed El Amine Monir[1] · Hadj Baltach[1] · Younes Mouchaal[2] · G. Murtaza[3]**

Received: 12 April 2017 / Accepted: 20 June 2017 / Published online: 15 July 2017


**Abstract** In this study, we have performed the first-principles investigation of the structural, electronic, magnetic, and optical properties of $TbNi_5$, $TbNi_3Ru_2$, and $TbNi_3Rh_2$ compounds. The full-potential linearized augmented plane waves with local orbitals method is used in the framework of density functional theory (DFT) employing the generalized gradient approximation (GGA) for the exchange correlation functional as implemented in WIEN2k package. The structural properties are reposed on the evaluation of the equilibrium lattice parameters of these compounds under hexagonal structure such as lattice constants ($a$ and $c$), bulk modulus ($B$), and its first pressure derivative ($B'$). The spin-polarized electronic structures, including band structure and density of states, are calculated employing the GGA plus band correlated Hubbard parameter (GGA+U) scheme. The results show that density of states and magnetic moment of the pure $TbNi_5$ compound are changed by doping. These changes are observed in the appearance of additional peaks on the spectral density of states (DOS) and in the augmentation of the total magnetic moment of $TbNi_3X_2$ (X = Ru and Rh) intermetallic compounds. Based on the electronic structure results, the frequency dependents of optical conductivity are estimated in all the spectra and interpreted in the interband optical absorption part.

**Keywords** $TbNi_5$ · FP-LAPW+lo · Electronic structure · Optical conductivity · GGA+U

## 1 Introduction

The $RNi_5$ intermetallic compound family (R is the rare-earth element) has a vast magneto-crystalline anisotropy, where it is caused by the crystal field interaction [1, 2], and large electronic structures; it crystallizes under the hexagonal system of the $CaCu_5$-type structure, which is described by the $P6/mmm$ space group. Actually, various electronic and experimental works have been extensively investigated on $RNi_5$ compounds and their substitutional derivatives, due to the existence of large-spectrum unusual physical properties and also due to the prospects of their exceptional applications in hydrogen storage technology and as adiabatic nuclear cooling agents [3–6], such as absorption capacity of hydrogen, observed in $LaNi_5$ compound with the formation of a hydride $LaNi_5H_{6,7}$ [7], the $ErNi_5$ compound which present a meta-magnetic from its ferromagnetic stable state. In some $RNi_5$ compounds, the magneto-caloric character is referred [8]. Through the litterature, we can mention the availability of the meta-magnetic even in paramagnetic $PrNi_5$ and ferromagnetic $ErNi_5$ compounds [9–12]. The magnetic properties of the $RNi_5$ compounds are obtained by the summarizing of three kinds of interactions: anisotropic interaction, spin-orbital interaction, and exchange interaction between the ion and the crystal field. The indirect exchange between $4f$ electrons in the conduction band gives

✉ G. Murtaza
murtaza@icp.edu.pk

Mohammed El Amine Monir
moniralpha29@gmail.com

[1] Laboratoire de Physique Quantique, de la Matière et de la Modélisation Mathématique (LPQ3M), Université de Mascara, 29000, Mascara, Algeria

[2] Laboratoire LPCMME, Université d'Oran 1, Ahmed Benbella, B.P. 1524 EL M'Naouer, 31000, Oran, Algeria

[3] Materials Modeling Lab, Department of Physics, Islamia College Peshawar, Peshawar, Pakistan

the magnetic aspect within $RNi_5$ systematic compounds. The ferromagnetic temperature ordering $T_C$ is estimated in the vicinity around 25 K [13].

The $RNi_5$ compounds have also been excessively studied with the use of experimental techniques like the measurements of the magnetization and the susceptibility [14, 15], heat capacity [16], X-ray magnetic circular dichroism [17], $\mu$SR spectroscopy [18], NMR spin echo [19], and elastic and inelastic neutron scattering [20–22]. The substitution of nickel atoms with other $p-$ or $d-$ metals exhibits substantial changes in most physical properties of $RNi_5$ intermetallic compounds. For example, nonmonotonic concentration dependences of magnetic [23, 24], electronic [24, 25], and crystalline [23, 26] are observed in the $TbNi_{5-x}Al_x$ system. Many works have been referred in the $TbNi_5$ group doping by the replacing of Ni with a nonmagnetic element such as Al, Ga, and Si [27–29]. In the other part, the substitution of nickel by a magnetic element (Fe or Co atoms) gives modifications in increasing Curie temperature ($T_C \approx 280$ K for $TbNi_4Fe$ and $T_C \approx 60$ K for $TbNi_4Co$) [30]. Important changes on the electronic structure and optical conductivity due to the influence of nonmagnetic Cu and Al have been deeply studied and referred availably in the literature [31, 32].

In this work, we have investigated the study of structural, electronic, magnetic, and optical properties of the pure $TbNi_5$ and their $TbNi_3Ru_2$ and $TbNi_3Rh_2$ derivative intermetallic compounds; the goal of this research is to show the role and the effect of the substitute transition metal (TM) on the electronic, magnetic, and optoelectronic properties of $TbNi_5$ compound.

The rest of the paper is ordered as follows: Section 2 exhibits brief descriptions of the calculation method. Section 3 gathers the obtained results and discussion of the structural, electronic, magnetic, and optical properties. In the end, the conclusions taken during this approach are summarized in Section 4.

## 2 Methodology

In this present approach, the projector full-potential augmented pane wave plus local orbitals (FP-L/APW+lo) [33, 34] has been performed within the first-principles calculations of the framework of density functional theory [35] and implemented in WIEN2k package [36] to give estimated results of structural, electronic, magnetic, and optical properties of pure $TbNi_5$ compound and their novel $TbNi_3Ru_2$- and $TbNi_3Rh_2$-derived alloys. In this work, we have used the optimized parameters as the muffin-tin sphere radii $R_{MT}$ are equal to 2.50, 2.24, 2.24, and 2.24 a.u. for Tb, Ni, Ru, and Rh, respectively. The plane wave–cutoff $R_{MT} \times K_{MAX}$ is chosen as 8, where $R_{MT}$ is the smallest muffin-tin (MT) sphere radius and $K_{MAX}$ is the greatest (maximum) modulus of vectors in the reciprocal lattice $\vec{K} = \vec{k} + \vec{G}$ of the first Brillouin zone (BZ). The mesh of $12 \times 12 \times 12$ Monkhorst-Pack scheme is generated by 135 special $k-$points which serve the integration in the first Brillouin zone. The energy convergence criterion for self-consistency is less than $10^{-4}$ eV. In fact, the valence electron configurations are considered as ($6s^2 4f^9$) for Tb, ($4s^2 3d^8$) for Ni, ($5s^1 4d^7$) for Ru, and ($5s^1 4d^8$) for Rh. The exchange-correlation potential is defined under the framework of generated gradient approximation of Perdew-Burke-Ernzerhof (GGA-PBE) [37]. The GGA approximation is applied to treat the structural properties whereas the electronic, magnetic, and optical properties of the herein compounds are examined by employing the GGA-PBE with on-site Hubbard term of Coulomb repulsion (PBE-GGA+$U$) [38–40]. The Hubbard correlation of direct and exchange (indirect) terms in the *4f*-shell of Tb was previously chosen as $U = 3.5$ eV and $J = 0.7$ eV [32]. The substitution of the nickel (Ni) by ruthenium (Ru) and rhodium (Rh), transition elements in $TbNi_5$ compound make the transition element at the crystallographic nonequivalent position of *2c*.

## 3 Results and Discussion

### 3.1 Structural Properties

The $TbNi_5$ compound is structured according to the hexagonal system of $CaCu_5$-type with *P6/mmm* symmetry space group (No. 191); the experimental lattice constants of this compound are found equal to $a = 4.892$ Å, and $c = 3.964$ Å [41].

According to the linear Birch-Murnaghan's equation of state (EOS) [42, 43], enunciated as the following expression, the total energy versus cell volume ($E - V$) curve was optimized in the goal to determine the equilibrium structural parameters in the stable state, such as lattice constants ($a_0$ and $c_0$), bulk modulus ($B$), its first pressure derivative ($B'$), and the minimum total energy ($E_0$).

$$E(V) = E(V) = a + bV^{-2/3} + cV^{-4/3} + dV^{-6/3} \quad (1)$$

where $V$ is the primitive cell volume and $a$, $b$, $c$, and $d$ are the optimized parameters.

The obtained results of the fitting equilibrium structural parameters of $TbNi_3X_2$ (X = Ni, Ru, and Rh) compounds are regrouped in Table 1, with other available experimental data and previous theoretical values inspired from the literature. The ($E - V$) curves for the three-alloys of $TbNi_3X_2$ are plotted and shown in Fig. 1, in which their graphs brand clearly the consistent minimum total energy of the system at the equilibrium for each compound. The comparison between our obtained structural results and experimental ones indicates a slight difference in the lattice constants observed for the case of $TbNi_5$ intermetallic compound, with an estimated rate of $-0.14\%$ for $a_0$, and of $-0.47\%$

**Table 1** The computed equilibrium structural parameters as lattice constants ($a_0$ and $c_0$), bulk modulus ($B_0$), and its pressure derivative ($B\prime$) of $TbNi_5$, $TbNi_3Ru_2$, and $TbNi_3Rh_2$ compounds, by employing the PBE-GGA approximation

| Compound | Lattice parameter $a_0$ (Å) | | | Lattice parameter $c_0$ (Å) | | | Bulk modulus $B_0$ (GPa) | | | $B'$ | | |
|---|---|---|---|---|---|---|---|---|---|---|---|---|
| | This work | Cal | Exp | This work | Cal | Exp | This work | Cal | Exp | This work | Cal | Exp |
| $TbNi_5$ | 4.887 | 4.872[a] | 4.894[b] | 3.947 | 3.966[a] | 3.966[b] | 160.18 | – | – | 4.95 | – | – |
| $TbNi_3Ru_2$ | 5.026 | – | – | 4.059 | – | – | 117.61 | – | – | 4.74 | – | – |
| $TbNi_3Rh_2$ | 5.041 | – | – | 4.085 | – | – | 174.55 | – | – | 3.99 | – | – |

[a]Ref. [44]

[b]Ref. [41]

for $c_0$, compared with measurement data. Furthermore, it is noticeable for the cases of other derivative compounds of $TbNi_5$ ($TbNi_3Ru_2$ and $TbNi_3Rh_2$) that the absence of the structural parameter data is an asset (advantage) to considering our results as a necessary reference to supplying further projects.

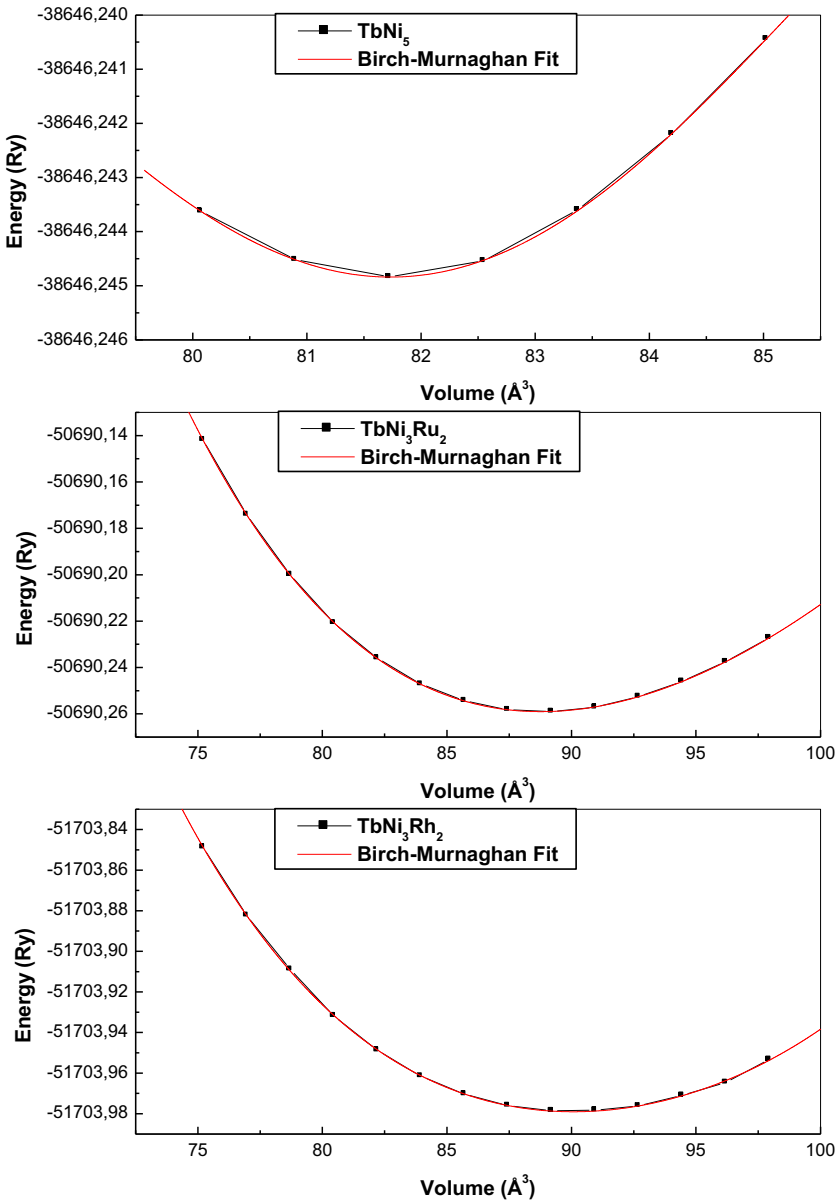


**Fig. 1** Total energy optimization as a function of primitive cell volume for $TbNi_5$, $TbNi_3Ru_2$, and $TbNi_3Rh_2$ intermetallic compounds

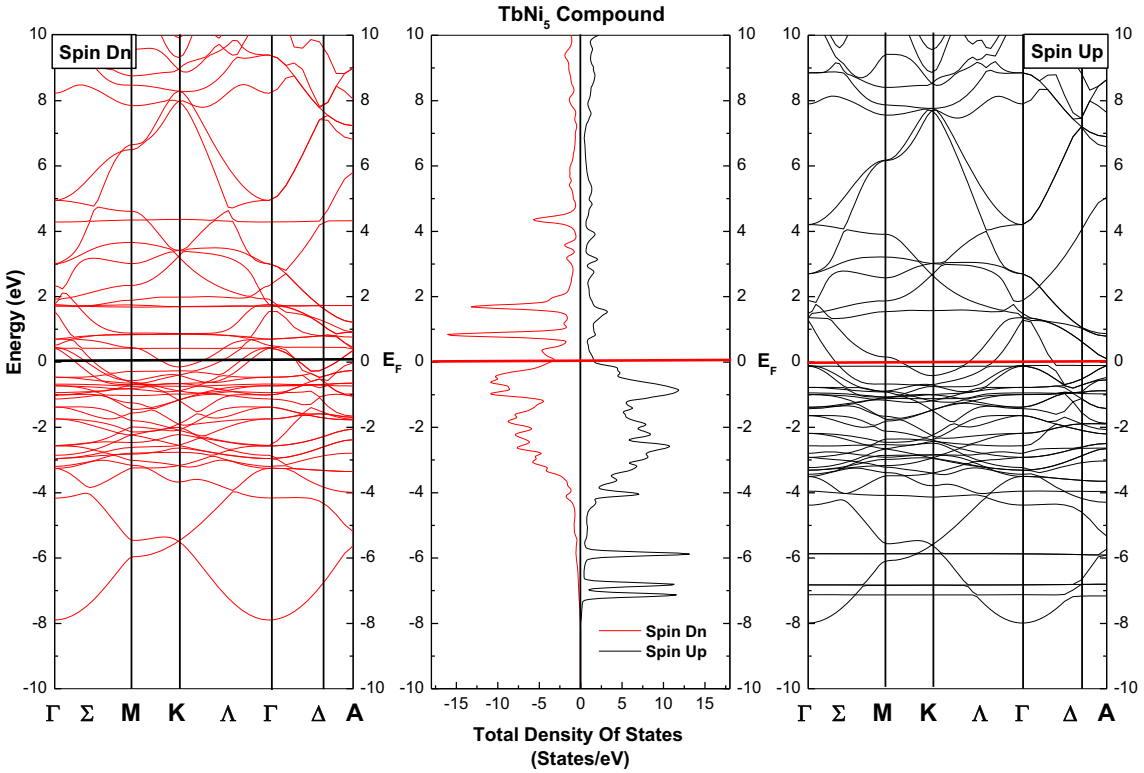


**Fig. 2** The obtained spin-polarized electronic band structure and total density of states (TDOS) of $TbNi_5$ intermetallic compound at their equilibrium lattice parameters, by employing PBE-GGA+U approximation

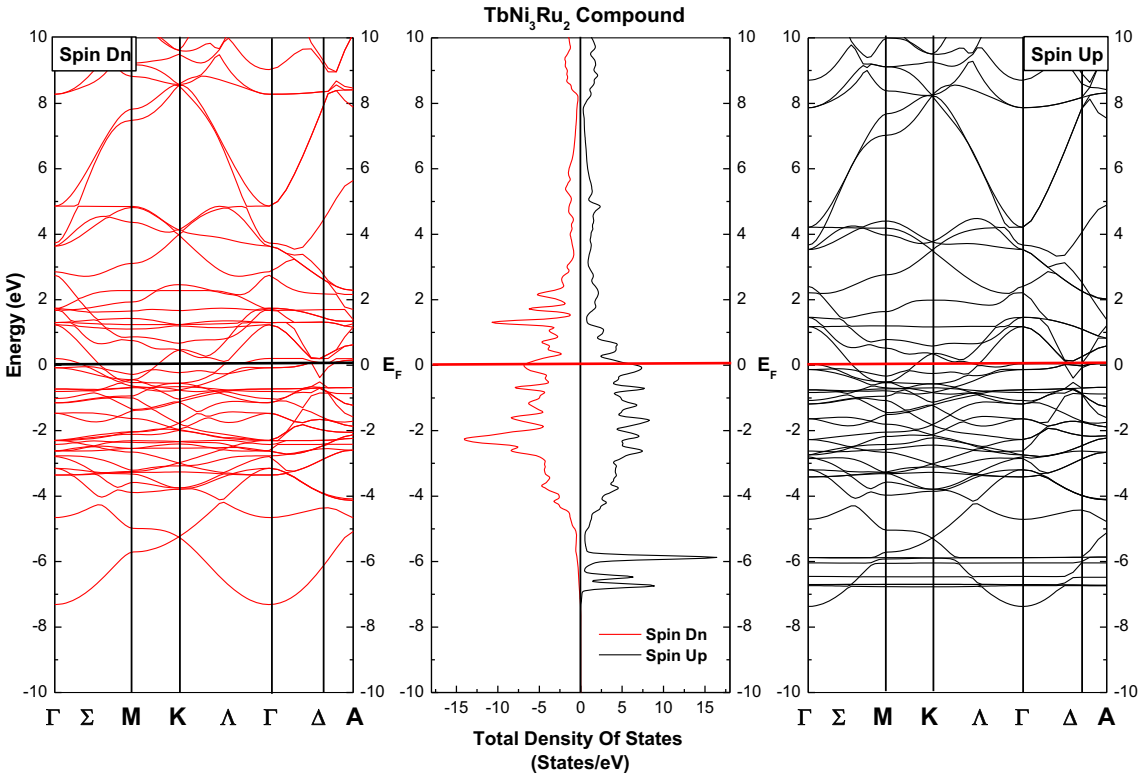


**Fig. 3** The obtained spin-polarized electronic band structure and total density of states (TDOS) of $TbNi_3Ru_2$ intermetallic compound at their equilibrium lattice parameters, by employing PBE-GGA+U approximation

### 3.2 Electronic Structure

#### *3.2.1 Band Structure*

The investigation on the electronic properties is useful to describe the electronic behavior of each material and classify the compounds in their true electronic category; the obtained results through the predicted or experimental methods will serve to give the appropriate potential use of the materials in technological devices. The calculated spin-polarized (spin-up, and spin-down) electronic band structures of hexagonal $TbNi_5$, $TbNi_3Ru_2$, and $TbNi_3Rh_2$ alloys are predicted under the framework of the PBE-GGA+U parameterization scheme, within their equilibrium lattice parameters presented in Table 1. Figures 2, 3, and 4 depict the band structures of $TbNi_5$, $TbNi_3Ru_2$, and $TbNi_3Rh_2$ compounds along the high-symmetry points in the first Brillouin zone (BZ) of the hexagonal system. It is obvious from these figures of all $TbNi_3X_2$ (X = Ni, Ru, and Rh) compounds that some energy bands go across the Fermi level ($E_F$) in both spin-up and spin-down directions, confirming the metallic nature of these alloys. Therefore, the remarkable effect of the transition element (TM = Ru, and Rh) substitutions is seen which modify the electronic structure of $TbNi_5$ compound by producing residual energy bands. The total densities of states (TDOS) curves are in perfect projection on their corresponding band structures which confirm the metallic behavior founding previously. Based on the TDOS plots of $TbNi_5$, $TbNi_3Ru_2$, and $TbNi_3Rh_2$ intermetallic compounds, the important $N(E)$ intensities are situated in the range of the valence band below $E_F$ (from −3.39 to 0 eV for $TbNi_5$, from −3.75 to 0 eV for $TbNi_3Ru_2$, and from −3.95 to 0 eV for $TbNi_3Rh_2$), where the specific part of $TbNi_5$ is principally filled by *3d*-Ni electrons of (*2c*) and (*3g*) sites, whereas the rest of the other two energetic condensed parts of $TbNi_3X_2$ compounds are contributed by both *3d*-Ni electrons of the (*3g*) site and *3d*-TM electrons of the (*2c*) site.

#### *3.2.2 Density of States*

To study the electronic structure of solids in detail, we must take our considerations to investigate on the electron density of states (DOS). The total and partial densities of states (TDOS and PDOS) projectors of the equilibrium $TbNi_3X_2$ (X = Ni, Ru, and Rh) alloys are calculated through the spin PBE-GGA+U approximation. The TDOS curves are presented in Figs. 2, 3, and 4, whereas the PDOS curves of $TbNi_5$, $TbNi_3Ru_2$, and $TbNi_3Rh_2$ are illustrated on Figs. 5, 6 and 7, respectively. The spin-dependent PDOS calculations of $TbNi_5$ show that the states of *3d*-Ni identified by the multi-peak structure are mainly located in the region between

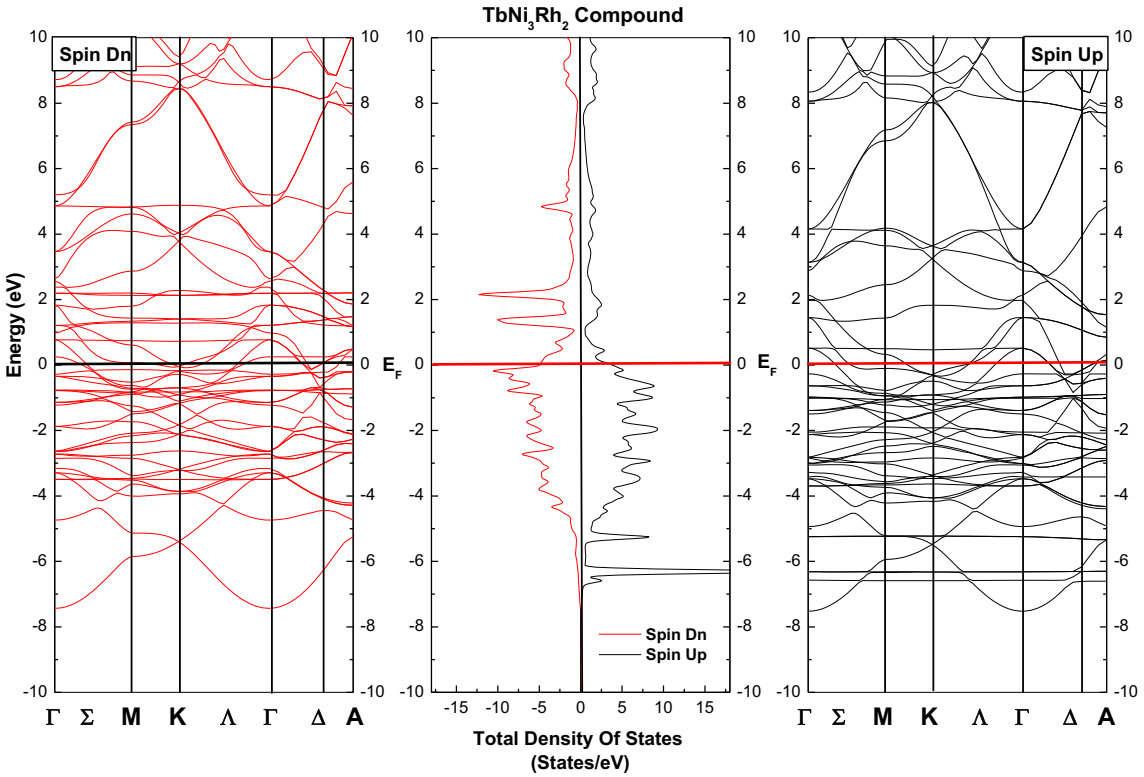


**Fig. 4** The obtained spin-polarized electronic band structure and total density of states (TDOS) of $TbNi_3Rh_2$ intermetallic compound at their equilibrium lattice parameters, by employing PBE-GGA+U approximation

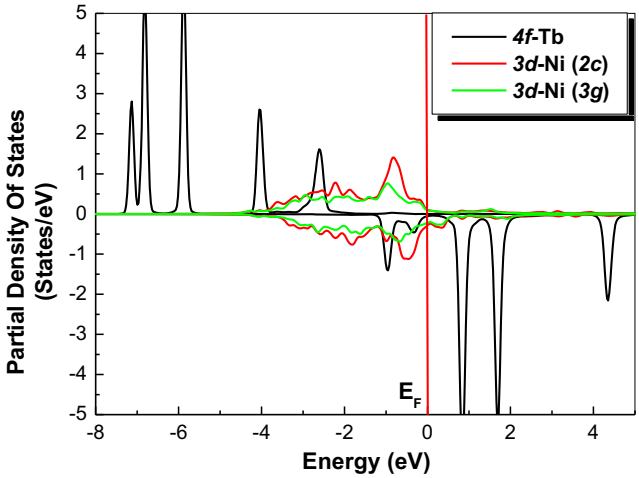


**Fig. 5** Spin-dependent partial densities of states of the equilibrium $TbNi_5$ compound, by using GGA+U scheme

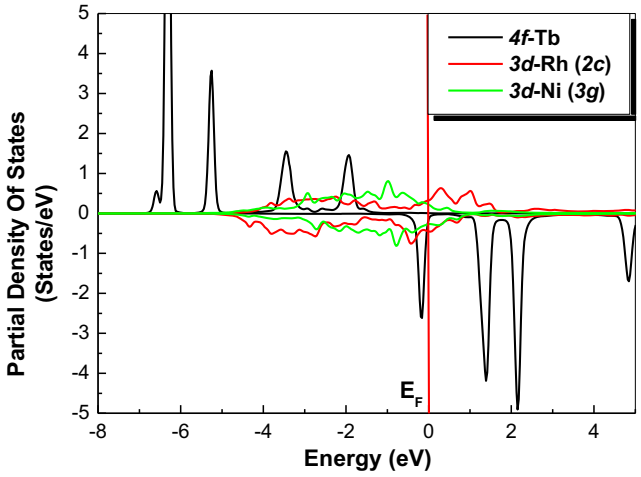


**Fig. 7** Spin-dependent partial densities of states of the equilibrium $TbNi_3Rh_2$ compound, by using GGA+U scheme

−4 eV and $E_F$, while the peaks around (−6.5 eV for spin-up projection and +1.1 eV for spin-down projection) belong to *4f*-Tb electrons. Moreover, intensive peaks of *4f*-Tb states are spotted at −5.92 and +0.95 eV for spin-up and spin-down cases, respectively, where this obtained result is agreeing in good matching with the other calculations [24, 25, 32]. According to Figs. 5 and 6 that show the PDOS curves of $TbNi_3Ru_2$ and $TbNi_3Rh_2$ compounds, the *3d*-TM (TM = Ru, and Rh) and *3d*-Ni contributions in both of their spin directions dominate the range from −5 to −1 eV for $TbNi_3Ru_2$ alloy and in the range from −5 to −2 eV for $TbNi_3Rh_2$ alloy, where a strong hybridization appears between these *3d*-TM and *3d*-Ni states along this filled part. The large exchange splitting between spin-up and spin-down electrons is referred to *4f*-Tb states, which gives an increase in the quantity of the magnetic moment, whereas spin exchange splitting corresponding to *3d*-Ni and –TM states are in weak evaluation. In both dependence PDOSs of $TbNi_3Ru_2$ and

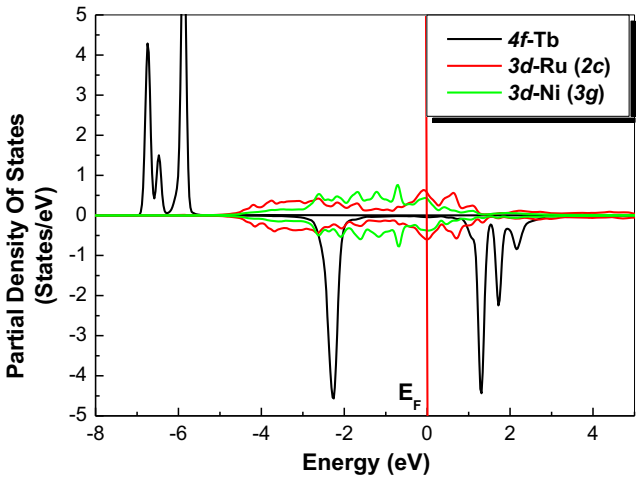


**Fig. 6** Spin-dependent partial densities of states of the equilibrium $TbNi_3Ru_2$ compound, by using GGA+U scheme

$TbNi_3Rh_2$, intense narrow peaks formed by *4f*-Tb states are situated in the broad energy region from −7 to −5 eV for the spin-up direction and from −2.5 to +2.15 eV for the spin-down direction. Furthermore, the impact of Ru and Rh substitute impurities for Ni in *2c* positions is focused on some deformations in the broad energy part between −5 eV and $E_F$, where their Ru and Rh bands are distributed in different manners comparing to the pure $TbNi_5$. It is noticeable that some summit peaks of *4f*-Tb states are reduced in the case of $TbNi_3Rh_2$, while some peaks of *4f*-Tb states disappear in the case of $TbNi_3Ru_2$. Also, it is lucidly observed that the TDOS intensities diminish when the Ru and Rh atoms replace the Ni atom in *2c* positions.

### 3.3 Magnetic Properties

#### *3.3.1 Magnetic Moment*

Systematic predictions of the magnetic properties of $TbNi_3X_2$ (X = Ni, Ru, and Rh) alloys within the GGA+U parameterization approximation were displayed in their sizes of total magnetic moments ($M_{Tot}$), local magnetic moments of Tb, Ni (*2c*), Ru (*2c*), Rh (*2c*), and Ni (*3g*) sites, and interstitial magnetic moments. The obtained values are listed in Table 2, wherein it is evident that the total magnetic moment for each compound mainly comprises the Tb contribution with weak magnetic moment quantities coming from other Ni, Ru, and Rh elements; this phenomenon is due to the wide splitting of *4f*-Tb states between both spin-up and spin-down directions. The local magnetic moments of each site have the same sign in parallel ordering, confirming the intrinsic ferromagnetic property of these compounds. Therefore, the hybridization between *3d*-Ni (*3g*) and *3d*-TM (*2c*) states is principally responsible for reducing the atomic magnetic moment of Ni (*3g*) and TM (*2c*) atoms from its free

**Table 2** The computed results of total magnetic moment ($M_{Tot}$ in $\mu_B$), atomic magnetic moment of each site in $TbNi_3X_2$ (X = Ni, Ru, and Rh) alloys, and magnetic moment in the interstitial region, by using the PBE-GGA+U approximation

| Alloy | Calculations | Magnetic moment ($\mu_B$) | | | | |
|---|---|---|---|---|---|---|
| | | Tb | Ni (*3g*) | X (*2c*) | Interstitial | Total |
| $TbNi_5$ | This work | 5.9303 | 0.3637 | 0.6204 | −0.1630 | 8.0993 |
| | Other cal. | 5.800[a] | 0.280[a] | 0.270[a] | – | – |
| | | 6[b] | 0.3[b] | 0.3[b] | – | – |
| | Exp. | 6[c] | 0.3[c] | 0.3[c] | – | – |
| $TbNi_3Ru_2$ | This work | 6.1064 | 0.0498 | 0.0030 | 0.0374 | 6.2992 |
| | Other cal. | – | – | – | – | – |
| | Exp. | – | – | – | – | – |
| $TbNi_3Rh_2$ | This work | 5.8768 | 0.2684 | 0.2277 | 0.0447 | 7.1822 |
| | Other cal. | – | – | – | – | – |
| | Exp. | – | – | – | – | – |

[a]Ref. [46]

[b]Ref. [47]

[c]Ref. [45]

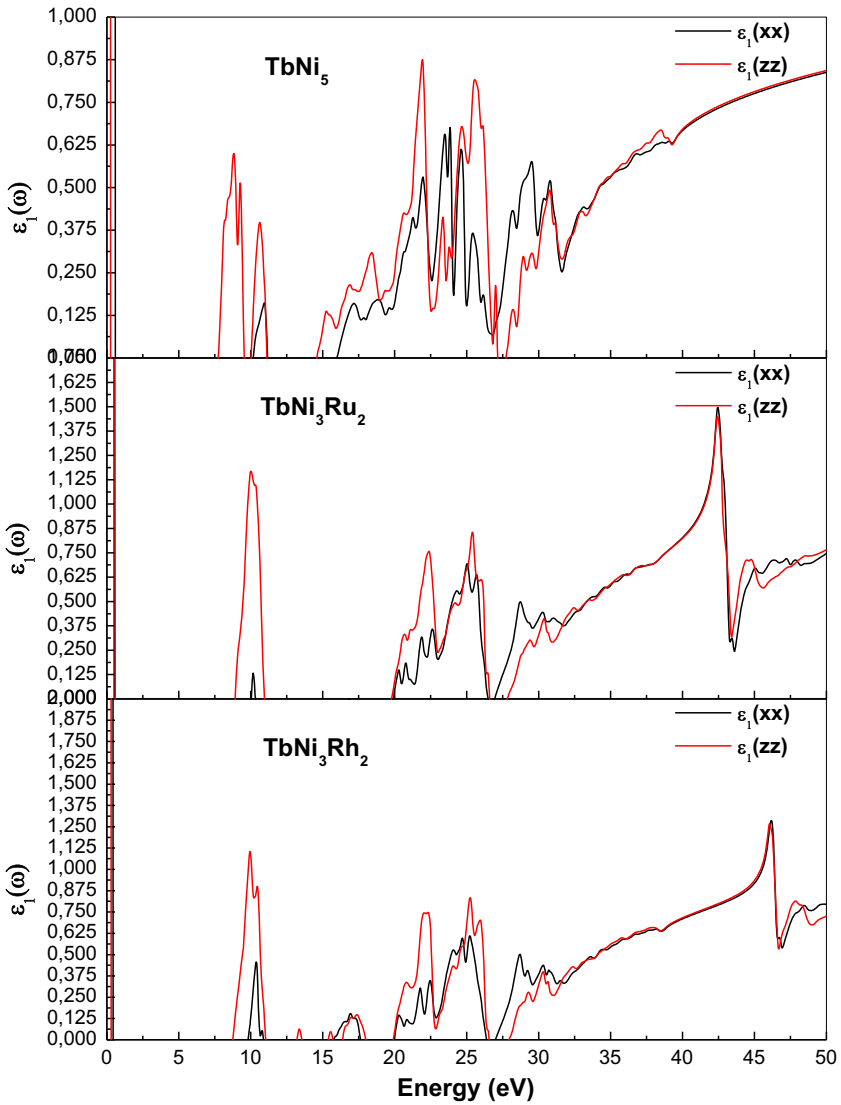


**Fig. 8** Real part of the dielectric function of $TbNi_5$, $TbNi_3Ru_2$, and $TbNi_3Rh_2$ intermetallic compounds

space charge value and also producing feeble local magnetic moments on the interstitial zone. The obtained magnetic moment results corresponding to the pure $TbNi_5$ intermetallic compound are in well concordance with the experimental data [45] available in the literature. Furthermore, the effects of the Ru and Rh atom substitutions for the Ni atom at *2c* positions within the pure $TbNi_5$ compound are collected to decrease the total magnetic moment of the system.

### 3.4 Optical Properties

#### *3.4.1 Dielectric Function*

The frequency-dependent complex dielectric function $\varepsilon\ (\omega)$ is a response of the substance which is useful for the optical properties of each system.

$$\varepsilon\ (\omega) = \varepsilon_1\ (\omega) + i\,\varepsilon_2\ (\omega) \tag{2}$$

where the real and the imaginary parts are dependent on each other by the Kramers-Kronig (KK) relation [48, 49]. The computed frequency dependent on the real $(\varepsilon_1)$ and imaginary parts $(\varepsilon_2)$ of $TbNi_3X_2$ (X = Ni, Ru, and Rh) in parallel $(E_{xx})$ and perpendicular $(E_{zz})$ directions of polarization, along the wavelength limit, is illustrated in Figs. 8 and 9, respectively. According to Fig. 2, the static dielectric constant $\varepsilon_1\,(0)$values are about 1.00, 1.78, and 1.76 for $TbNi_5$, $TbNi_3Ru_2$, and $TbNi_3Rh_2$ alloys, respectively. The existence of multi-peaks situated in the energy region between 15 and 35 eV and around 10 eV in the case of the pure $TbNi_5$ compound also can be seen. Due to the impact of Ru and Rh transition metal substitutes, the intensities of these peaks are progressed in their energy ranges. Moreover, other peaks are located at 41 eV for $TbNi_3Ru_2$ and for $TbNi_3Rh_2$. The increasing of the peak summit is observed in TM-doped $TbNi_5$ alloys, explaining the strong

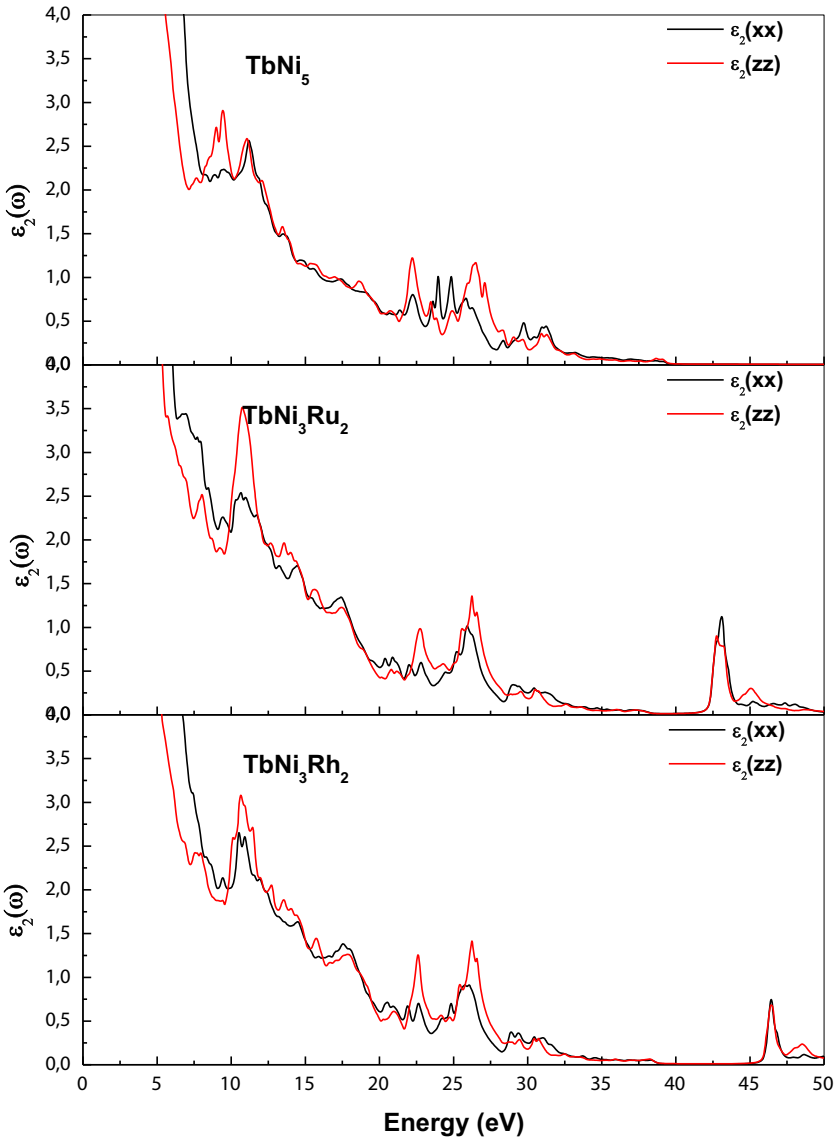


**Fig. 9** Imaginary part of the dielectric function of $TbNi_5$, $TbNi_3Ru_2$, and $TbNi_3Rh_2$ intermetallic compounds

energy absorption character. Additionally, it is evident that the highest peak is referred in $\varepsilon_1(zz)$ around 21 eV for the case of $TbNi_5$ compound, whereas the spotting of both $\varepsilon_1(xx)$ and $\varepsilon_1(zz)$ highest peaks are at 41 eV for $TbNi_3Ru_2$ compound and at 46 eV for $TbNi_3Rh_2$ compound.

Imaginary parts of the dielectric function of $TbNi_5$, $TbNi_3Ru_2$, and $TbNi_3Rh_2$ compounds are shown in Fig. 9; in fact, we remark that their curves decrease with the change of the photon energy from lower to higher, where this shift showed pronounced peaks in the cases of $TbNi_3Ru_2$ and $TbNi_3Rh_2$ compounds comparing to the pure $TbNi_5$ compound, demonstrating the increasing of the absorption ranges of these TM-doped $TbNi_5$ alloys. Moreover, these imaginary part of the curves decreases drastically from the highest values which are situated in the infrared region. Furthermore, the effect of transition metal (TM) doping in *2c* positions creates a small peak with low intensity in both parallel ($E_{xx}$) and perpendicular ($E_{zz}$) polarizations around 43 and 46 eV for $TbNi_3Ru_2$ and $TbNi_3Rh_2$ compounds, respectively.

### *3.4.2 Reflectivity*

The complex refractive index is defined as $N(\omega) = n(\omega) + i\,k(\omega)$, where $n(\omega)$ and $k(\omega)$ are the real and imaginary parts of the complex refractive index, which are related to $\varepsilon(\omega)$ by the following relations:

$$n(\omega) = \left(\frac{\sqrt{\varepsilon_1^2+\varepsilon_2^2}+\varepsilon_1}{2}\right)^{1/2}, k(\omega) = \left(\frac{\sqrt{\varepsilon_1^2+\varepsilon_2^2}-\varepsilon_1}{2}\right)^{1/2} \quad (3)$$

With the knowledge of $n(\omega)$ and $k(\omega)$, it is obvious to determine the percentage of reflectivity of solids at normal incident of electromagnetic wave, which is estimated by the

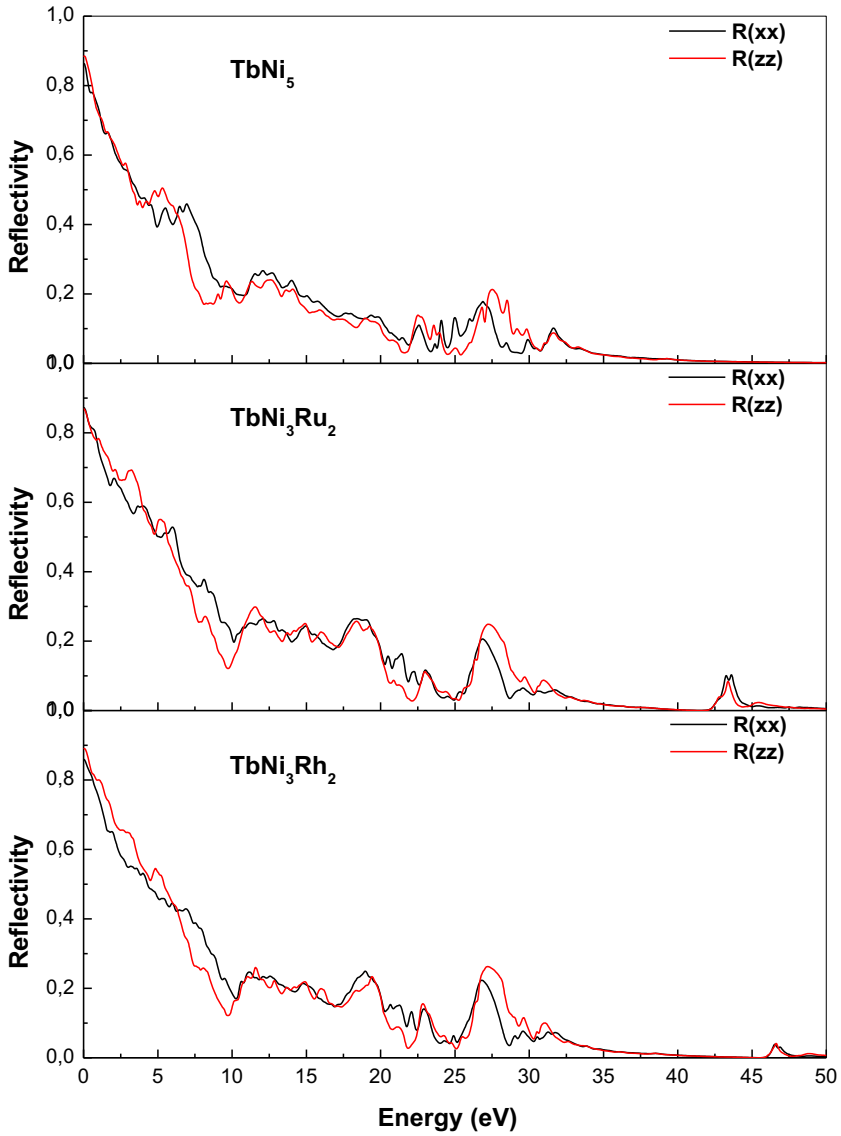


**Fig. 10** Reflectivity of $TbNi_5$, $TbNi_3Ru_2$, and $TbNi_3Rh_2$ intermetallic compounds

ration of the refracted on the incident energies of photon. It is given as follows:

$$R\ (\omega) = \frac{(n-1)^2 + k^2}{(n+1)^2 + k^2} \tag{4}$$

We have computed the estimated reflectivity $R\,(\omega)$ through the availability of frequency-dependent real and imaginary parts of the dielectric function for both $E_{xx}$ and $E_{zz}$ polarizations. Figure 10 depicts the evolution of $R\,(\omega)$ versus photon energy; we can see that their graphs decrease from the lower (infrared region) to the higher energy regions, where the highest reflectivity values of all $TbNi_5$, $TbNi_3Ru_2$, and $TbNi_3Rh_2$ compounds are located in the infrared region ($E$ ~0 eV) about 88, 86, and 89%, respectively; this decrease of $R\,(\omega)$ is explained by the enhancement of the absorption part in the dielectric function. It is noticeable that the reflectivity $R\,(\omega)$ is strongly related to the imaginary part of the dielectric function, because their curves are rigorously similar. In the region from 5 to 35 eV, the reflectivity peaks of TM-doped $TbNi_5$ are more pronounced than those of the pure $TbNi_5$, which are original from the inter-band interactions, where the reflectivity energy intervals of all the three compounds are the same; their highest intensities are focused in the infrared part and in the first fragment of the visible part of the spectrum. Moreover, the TM (Ru and Rh) substitutions on the $TbNi_5$ system present a slight change in the height of peaks, comparing to the pure $TbNi_5$.

### *3.4.3 Absorption Coefficient*

The absorption coefficient is a quantity that translates the response of the system under the effect of excitation. It is given in dependence with the dielectric function according to the following formula:

$$\alpha\ (\omega) = \frac{2\omega\, k(\omega)}{\hbar c} \tag{5}$$

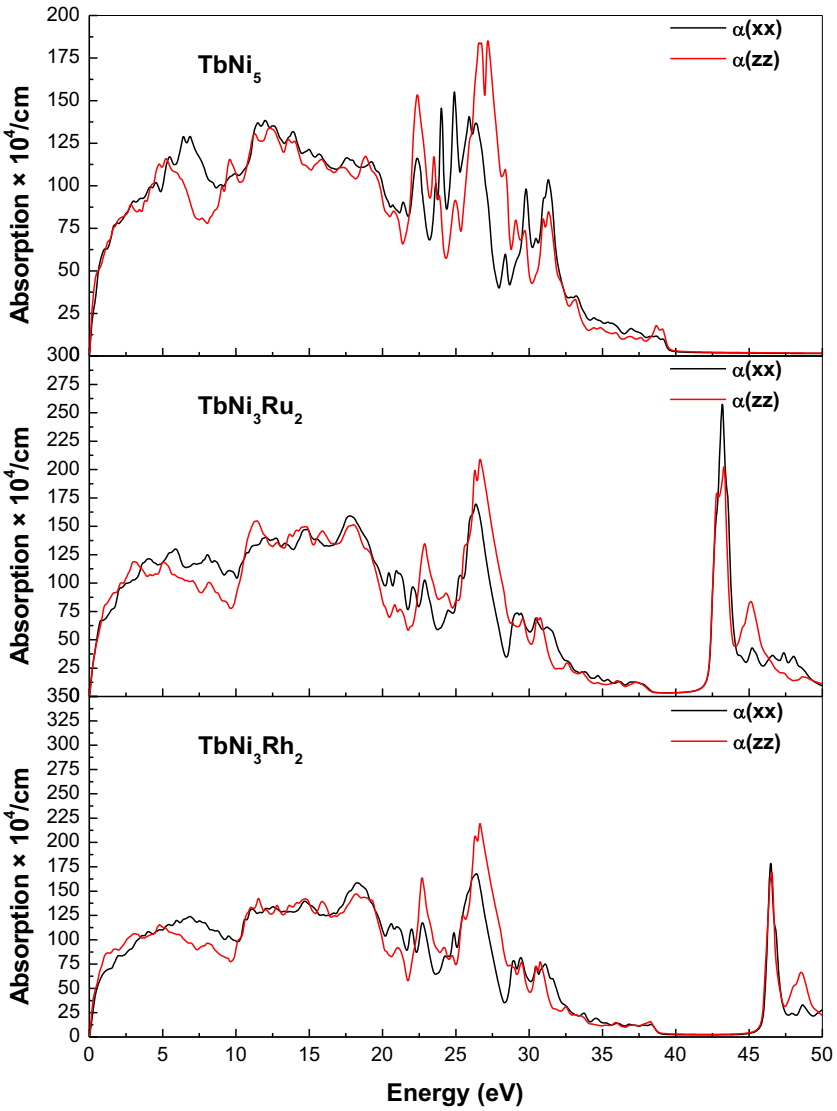


**Fig. 11** Absorption coefficient of $TbNi_5$, $TbNi_3Ru_2$, and $TbNi_3Rh_2$ intermetallic compounds

where it is fully linked to the imaginary part of the dielectric function.

Here, $c$ is the light speed in vacuum and $\omega$ is the energy unit.

The absorption coefficient of $TbNi_3X_2$ (X = Ni, Ru, and Rh) is reported in Fig. 11 showing the behavior of the both parallel ($E_{xx}$) and perpendicular ($E_{zz}$) polarization cases. Therefore, it is observed for all the three $TbNi_5$, $TbNi_3Ru_2$, and $TbNi_3Rh_2$ alloys that the absorption coefficient $\alpha$ ($\omega$) of $E_{xx}$and $E_{zz}$ increases from a less value in the energy part from 0 to 20 eV; after this region, due to the interband interactions, many multi-peaks have been formed in the energy range between 20 and 35 eV; finally, the curves decrease to attain zero intensity in the proximity of 40 eV. The sharp peak is observed for $E_{zz}$ around 27.5 eV for the pure $TbNi_5$, interpreting the top absorption of the light in this frequency point. The highest value of the absorption coefficient of TM-doped $TbNi_5$ is localized at 42.5 eV for $E_{xx}$of $TbNi_3Ru_2$ and at 27 eV for $E_{zz}$of $TbNi_3Rh_2$.

It is noticeable that the energy ranges of absorption of both TM-doped $TbNi_5$ alloys are widely expanded on the full energy spectrum with a width upper than of the pure $TbNi_5$ compound. The major impact of the impurity TM within $TbNi_5$ system is reported in the apparition of isolated sharp peaks in the ultraviolet spectrum around 42.5 and 47.5 eV for $TbNi_3Ru_2$ and $TbNi_3Rh_2$ compounds, respectively.

### *3.4.4 Optical Conductivity*

The optical conductivity is defined as a factor which describes the nature of the frequency dependence and the intensity of the reflecting medium as optical response. It has been given under the following formula:

$$\sigma\ (\omega) = n(\omega)\alpha(\omega)\frac{\omega}{2\pi} \tag{6}$$

where $n$ ($\omega$) and $\alpha$ ($\omega$) are refractive index and absorption coefficient, respectively.

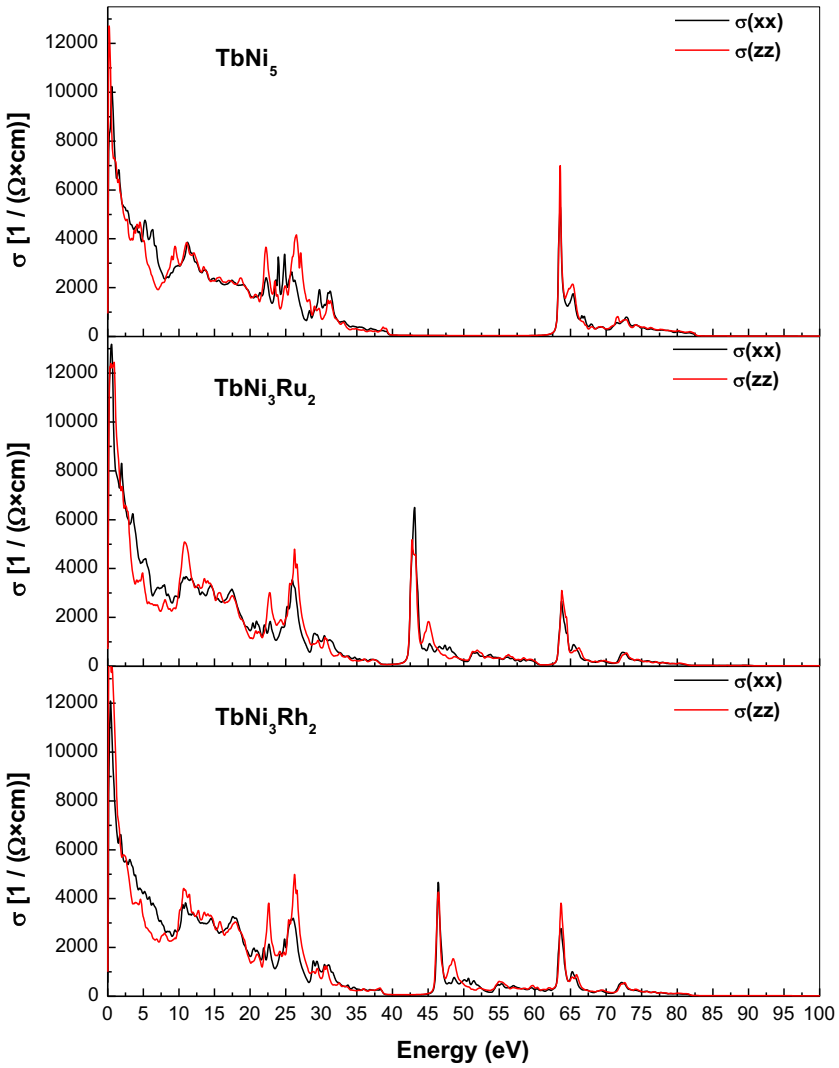


**Fig. 12** Optical conductivity of $TbNi_5$, $TbNi_3Ru_2$, and $TbNi_3Rh_2$ intermetallic compounds

The optical conductivity spectra $\sigma(\omega)$ of the pure $TbNi_5$ compound and their $TbNi_3Ru_2$ and $TbNi_3Rh_2$ alloys are shown in Fig. 12 along the photon energy. A violent enhancement is observed for the three compounds at the lower energy range of the infrared spectrum, which forms the sharpest peak, explained by the Drude rise (mechanism of interaction between electromagnetic waves and conduction electrons). Above $\hbar\omega$ ˜0.5 eV, the $\sigma(\omega)$ behavior of all the compounds decreases abruptly versus the increasing of the optical frequency $\sigma(\omega)$; this increasing is accompanied by the creation of multi-peaks which are due to the interband interactions. Then, the $\sigma(\omega)$ curve reaches zero intensity at 40 eV for the $TbNi_5$ compound, while some intense peaks appear in the energy range close to 42.5 eV for $TbNi_3Ru_2$ alloy and 46 eV for $TbNi_3Rh_2$ alloy, showing the effect of the inter-band absorption of light in these photon frequencies. It is obvious to mention that our obtained $\sigma(\omega)$ results of $TbNi_5$ case agree in well matching with the previous theoretical data [50]. Moreover, the introducing by substitution of the TM (Ru and Rh) element makes shifts in the optical conductivity dispersion $\sigma(\omega)$; in fact, multi-peaks are more pronounced in the range from 25 to 30 eV; other peaks become intensively reduced in the ultraviolet spectrum around 65 eV, comparing to the pure $TbNi_5$ intermetallic compound.

## 4 Conclusions

To sum up, in this study, we have performed the GGA and GGA+U calculations of the structural, electronic, magnetic, and optoelectronic properties of TM-doped $TbNi_5$ (TM = Ru and Rh) compounds, by using the first-principles FP-L/APW+lo method within the framework of the DFT theory. Therefore, in this approach, we have shown the role of the transition metal TM substitutions for nickel in *2c* positions proclaims changes on the electronic, magnetic, and optoelectronic properties of the pure $TbNi_5$ compound. Our obtained results of equilibrium parameters of $TbNi_5$ system are consistent with the available experimental data and theoretical values. The effect of doping Ru and Rh elements on the system ($TbNi_5$) depicts more modifications on the electronic structure, which are specified by production of novel reported peaks at the level of density of states (DOS) spectrum, confirming the metallic behavior of the three intermetallic compounds. The total and atomic magnetic moments are also evaluated; their results present fewer differences with those of the $TbNi_5$ parent, where the total magnetic moment is principally contributed by Tb atom. In the optoelectronic properties, the impact of the TM doped $TbNi_5$ system is characterized by great energy of absorption, apparition of isolated sharp peaks of absorption coefficient in the ultraviolet spectra, and pronounced peaks spotted in both reflectivity and absorption spectra, where these rises are significantly explained by the interband interactions. Moreover, the absorption bandwidths of $TbNi_3Ru_2$ and $TbNi_3Rh_2$ are more broadened on the light spectrum. In the end, the optical conductivity dispersion was predicted in reasons of comparing and interpreting the experimental results of the pure $TbNi_5$ system, demonstrating that the $\sigma(\omega)$ allure of the three alloys is lucidly interpreted by their corresponding calculations of the density of states.

## References


1. Romaka, V.V., Marciniak, B., Romaka, L., Gorelenko, Y., Pavlyuk, V.: J. Alloy. Comp. **493**, L12–L14 (2010)
2. Kuchin, A.G., Ermolenko, A.S., Khrabrov, V.I., Kourov, N.I., Makarova, G.M., Belozerov, Y.V., Lapina, T.P., Kulikov, Y.A.: J. Magn. Magn. Mater. **29**, 238 (2002)
3. Trémolet de Lacheisserie, E., Gignoux, D., Schlenker, M.: Magnetism: Materials and Applications. Springer, Berlin (2005)
4. Gschneidner, K.A., Pecharsky, V.K., Tsokol, A.O.: Rep. Progr. Phys. **68**, 1479 (2005)
5. Mushnikov, N.V.: Phys. Uspekhi **55**, 421 (2012)
6. Coey, J.M.D.: Magn. IEEE Trans. **47**, 4671 (2011)
7. Senoh, H., Takeichi, N., Takeshita, H.T., Tanaka, H., Kiyobayashi, T., Kuriyama, N.: Hydrogenation properties of RNi5 (R: rare-earth) intermetallic compounds with multi pressure plateaux. Mater. Trans. **44**, 1663–1666 (2003)
8. Ranke, P.J., Mota, M.A., Grangeia, D.F., Magnus, A., Carvalho, G., Gandra, F.C.G., Coelho, A.A., Caldas, A., Oliveira, N.A., Gama, S.: Magnetocaloric effect in the *R*Ni5 ($R$ = Pr, Nd,Gd, Tb, Dy, Ho, Er) series. Phys. Rev. B: Condens. Matter Mater. Phys. **70**, 134428 (2004)
9. Radwański, R.J., Kim-Ngan, N.H., Kayzel, F.E., Franse, J.J.M., Gignoux, D., Schmitt, D., Zhang, F.Y.: The specific heat of $ErNi_5$ and $LaNi_5$. J. Phys.: Condens. Matter **4**, 8853–8862 (1992)
10. Kayzel, F.E.M., Franse, J.J., Radwański, R.J.: High field magnetization and specific heat of $ErNi_5$. IEEE Trans. Magn. **30**, 890–892 (1994)
11. Gignoux, D., Schmitt, D.: Commensurability versus incommensurability in rare earth intermetallic compounds. J. Magn. Magn. Mater. **129**, 53–58 (1994)
12. Gignoux, D., Schmitt, D.: Metamagnetism and complex magnetic phase diagrams of rare earth intermetallics. J. Alloys Compd. **225**, 423–431 (1995)
13. Kuchin, A.G., Ermolenko, A.S., Khrabrov, V.I., Kourov, N.I., Makarova, G.M., Belozerov, Y.V., Lapina, T.P., Kulikov, Y.A.: J. Magn. Magn. Mater. **238**, 29 (2002)
14. Gignoux, D., NaitSaada, A., de la Bathie, R.P.: Magnetic properties of TbNi and HoNi single crystals. J. Phys. Colloq. **40**(C5), 188–190 (1979)
15. Grechnev, G.E., Desnenko, V.A., Panfilov, A.S., Svechkarev, I.V., Brommer, P.E., Franse, J.J.M., Kayzel, F.E.: Pressure effect on electronic structure and magnetic properties of RNi5. Phys. B **237–238**, 532–533 (1997)
16. Svoboda, P., Vejpravova, J., KimNgan, N.T.H., Kaysel, F.J.: Specific heat study of selected RNi5. J. Magn. Magn. Mater. **272–276**, 595–596 (2004)
17. Galera, R.M., Rogalev, A.: Hard X-ray magnetic circular dichroism in GdNi5 and TbNi5 single crystals. J. Appl. Phys. **85**, 4889–4891 (1999)

18. de Reotier Dalmas, P., Yaouanc, A., Gubbens, P.C.M., Gignoux, D., Gorges, B., Schmitt, D., Hartmann, O., W¨appingm, R., Weidinger, A.: Effect of Tb3+ crystal field on the positive muon precession frequency in TbNi5. J. Magn. Magn. Mater. **104–107**, 1267–1268 (1992)
19. Carboni, C., Gignoux, D., Li, Y., Ross, J.W., Tary, A.: The field dependence of the hyperfine splitting of terbium in $TbNi_5$. J. Phys.: Condens. Matter **8**, 1763–1774 (1996)
20. Goremychkin, E.A., Muhle, E., Ivanitski, P.G., Krotenko, V.T., Pasechkin, M.V., Slisenko, V.V., Vasilkevich, A.A., Lippold, B., Chistyakov, O.D., Savitski, E.M.: Crystal electric field splitting in $TbNi_5$ and $ErNi_5$ studied by inelastic neutron scattering. Phys. Status Solidi B **121**, 623–631 (1984)
21. Gignoux, D., Rhyne, J.J.: Spin excitations in TbNi5 by inelastic neutron scattering. J. Magn. Magn. Mater. **54–57**, 1179–1180 (1986)
22. Lemaire, R., Paccard, D.: Structure magnétique du composé intermétallique TbNi5. C. R. Acad. Sci. B (Paris) **270**, 1131–1133 (1970)
23. Kuchin, A.G., Ermolenko, A.S., Khrabrov, V.I., Kourov, N.I., Makarova, G.M., Belozerov, Y.V., Lapina, T.P., Kulikov, Y.A.: J. Magn. Magn. Mater. **238**, 29 (2002)
24. Burzo, E.: Rom. Rep. Phys. **59**, 337 (2007)
25. Burzo, E., Takacs, A., Neumann, M., Chioncel, L.: Phys. Status Solidi C **1**, 3343 (2004)
26. Blazina, Z., Sorgi, B., Drăsner, A.: J. Phys.: Condens. Matter **9**, 3099 (1997)
27. Burzo, E., Takàcs, A., Neumann, M., Chioncel, L.: Phys. Status Solidi (c) **1**, 3343 (2004)
28. Lizárraga, R., Bergman, A., Björkman, T., Liu, H.P., Andersson, Y., Gustafsson, T., Kuchin, A.G., Er_molenko, A.S., Nordström, L., Eriksson, O.: Phys. Rev. **B74**, 094419 (2006)
29. Falkowski, M., Andrzejewski, B., Kowalczyk, A.: J. Alloys Compd. **442**, 155 (2007)
30. Haldar, A., Dhiman, I., Das, A., Suresh, K.G., Nigam, A.K.: J. Alloys Compd. **509**, 3760 (2011)
31. Nekrasov, I.A., Kokorina, E.E., Galkin, V.A., Kuzmin, Y.u.I., Knyazev, Y.u.V., Kuchin, A.G.: Phys. B **407**, 3600 (2012)
32. Knyazev, Y.u.V., Lukoyanov, A.V., Kuz′min, Y.u.I., Kuchin, A.G.: Phys. Solid State **55**, 385 (2013)
33. Wong, K.M., Alay-e-Abbas, S.M., Shaukat, A., Fang, Y., Lei, Y.: J. Appl. Phys. **113**, 014304 (2013)
34. Wong, K.M., Alay-e-Abbas, S.M., Fang, Y., Shaukat, A., Lei, Y.: J. Appl. Phys. **114**, 034901 (2013)
35. Hohenberg, P., Kohn, W.: Phys. Rev. **136**, B864 (1964)
36. Blaha, P., Schwarz, K., Sorantin, P., Trickey, S.K.: Comput. Phys. Commun. **59**, 339 (1990)
37. Perdew, J.P., Burke, S., Ernzerhof, M.: Phys. Rev. Lett. **77**, 3865 (1996)
38. Novak, P., Kunes, J., Chaput, L., Pickett, W.E.: Phys. Status Solidi B **243**, 563 (2006)
39. Anisimov, V.I., Solovyev, I.V., Korotin, M.A., Czyzyk, M.T., Sawatzky, G.A.: Phys. Rev. B **48**, 16929 (1993)
40. Petukhov, A.G.: Phys. Rev. B **67**, 153106 (2003)
41. Buschow, K.H.J.: Rep. Prog. Phys. **40**, 1179 (1977)
42. Murnaghan, F.D.: Proc. Natl. Acad. Sci. USA **30**, 5390 (1944)
43. Shang, S.L., Wang, Y., Kim, D., Liu, Z.-K.: Mater. Comput. Sci. **47**, 1040 (2010)
44. Goraus, J., Malankiewicz, P.: Acta Phys. Polon. **121**, 1077 (2012)
45. Haldara, A., Dhimanb, I., Dasb, A., Suresha, K.G., Nigamc, A.K.: J. Alloys Compd. **509**, 3760–3765 (2011)
46. Knyazev, Y.V., Kuz'min, Y.I., Kuchin, A.G., Lukoyanov, A.V., Nekrasov, I.A.: Opt. Spectrosc. **104**, 3 (2008)
47. Knyazev, Y.V., Lukoyanov, A.V., Kuz'min, Y.I., Haldar, A., Suresh, K.G.: Opt. Spectrosc. **117**, 3 (2014)
48. Mahan, G.D.: Many Particle Physics. Plenum Press, New York (1990)
49. Dressel, M., Gruner, G.: Electrodynamics of Solids. Cambridge University Press, Cambridge (2002)
50. Knyazev, Y.V., Lukoyanov, A.V., Kuz'min, Y.I., Kuchin, A.G.: Phys. Solid State **55**, 2 (2013)